Prediction of Detonation-Induced Disturbances Propagating Upstream into Inlets of Rotating Detonation Combustors

Alexander Feleo*, Joshua Shepard†, and Mirko Gamba‡
University of Michigan, Ann Arbor, MI 48109

Disturbances caused by the detonation wave in a rotating detonation combustor (RDC) propagate upstream through the inlet, and can potentially affect and couple to upstream components, such as turbomachinery or isolators. These disturbances can potentially also affect the operation of the RDC itself. By drawing from the analogy of a detonation wave bounded by an inert gas, the pressure disturbances observed upstream of the inlet are explained as the consequence of the passage of an upstream propagating oblique shock. In this study, the pressure rise in the plenum from the oblique shock is measured in an axial air inlet RDC. The speed of the upstream propagating wave is estimated to be moderately above the acoustic speed of the oxidizer in the plenum. The wave propagates into the plenum despite local regions of choking in the inlet. It is estimated that the time it takes a fluid particle to transit from the plenum to the detonation channel through the inlet is much larger than the rotational time of the detonation wave. This implies that a fluid particle experiences multiple shocks prior to entering the detonation channel. The oblique shock propagating upstream through the inlet area change is modeled by leveraging an analogy with a quasi-1D shock wave moving in a variable area duct with mean (incoming) flow. Due to flow expansion along the area change, fluid particles are found to experience stronger shocks in the inlet than in the plenum, thereby creating different thermodynamic states within the fill region as the oxidizer emerges from the inlet.

I. Introduction

Detonation-based devices may allow for additional work to be extracted compared to traditional deflagration based devices. A rotating detonation engine (RDE) is one such device, in which a detonation continuously propagates around an annulus as the flow exits the annulus axially. One of the effects of the propagation of the detonation wave is the momentary flow blockage of the injectors due to the pressure rise across the wave. Once the injectors recover, fresh reactants are injected and then consumed by the next detonation wave. While simple to design from a systems standpoint, the understanding of the operation, flow-field, and performance of these devices experimentally, thus far, have strayed from the conventional theory. In addition to not fully understanding these observed non-ideal phenomenons, translating laboratory testing into a larger system with integration of turbo-machinery for power generation or shock trains for high-speed flight, is not well understand. These technical questions have thus far prevented this style of propulsion from seeing real-world use.

Quantifying and demonstrating pressure gain from using a rotating detonation combustor (RDC) has been the focus of the RDE community for the past few years.[1–5] Thus far pressure gain has not been demonstrated experimentally. One of the primary sources of being theorized is the pressure drop across the injectors.[6] Thus, to achieve the promised pressure gain, the need for low-loss injectors, with more open throat areas, is paramount. The more open throats have been seen to decrease the pressure loss across the system.[4] However, by opening up the injector throat there is the potentially significant cost of increasing the coupling between the fuel and oxidizer plenums and the detonation channel. This coupling has been examined in

*Graduate Research Assistant, Dept. of Aerospace Engineering.
†Graduate Research Assistant, Dept. of Aerospace Engineering.
‡Associate Professor, Dept. of Aerospace Engineering, AIAA member.

some previous experimental works[7,8]and numerical works.[9] In a practical system, the plenum/inlet of a RDC would be coupled to a compressor or an isolator which may be sensitive to back-pressurization events that may become stronger with more open throats. Quantifying and understanding the response of the injectors and what enters the plenums is then imperative if such devices are going to see real-world use. This work will seek to utilize experimental measurements and a simplified flowfield representation to better understand the changes in dynamics brought about by changing the oxidizer inlet area. Specifically, the unsteady pressure feedback into the plenum is explored in the context of an upstream propagating oblique shock generated by the detonation being bounded by the oxidizer in an axial-air inlet RDC.

II. Experimental Setup

A. Description of RDC

Testing was performed on a 154 mm (6.06") round RDC with a 7.6 mm (0.3") annulus gap, combustor length of 115 mm (4.53"), and no exit constriction. A modified version of axial air inlet injectors considered in the past[11] was used to inject the fuel/air. The general configuration is shown in Figure 1 since it is similar to our legacy axial air inlet (AAI-1) injector, though the air and fuel flowpaths are more judiciously designed to manage some of the non-idealities observed in our legacy injector. This combustor can have different inlet throat areas without significantly altering the aerodynamic characteristics in the throat. Here we will consider a ratio between the channel and air inlet throat area (A_{ch}/A_{th}) of 3 and 4.

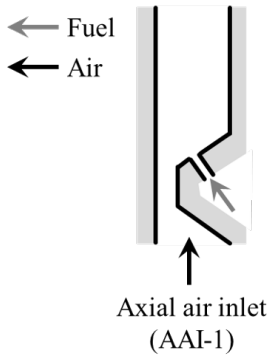

Figure 1. Diagram of air inlet / fuel injection scheme tested in this work. See also Shepard et al.[10]

High-speed pressure measurements, aft high-speed chemiluminescent video, and low-speed static pressure measurements via continuous tube attenuated pressure (CTAPs) in the channel are applied to investigate the operation of the system similar to our previous work.[12,13] The standard arrangement of sensors for these tests considered in this study is shown in Figure 2 in which the dotted lines are the injection plane and exit plane of the combustor. The high-speed pressure measurements in the detonation channel (EWCTV-312 Kulites) are aligned azimuthally but are spaced apart axially by 60 mm (2.35"). To study the dynamics of the extended plenum, two high-speed pressure measurements (XTEL-190 Kulites) were added to the plenum. These were at the same axial location but clocked 90° apart to distinguish between rotating and pulsing waves. These measurements are taken about 89 mm (3.5") from the injectors. In addition to the high-speed measurements, CTAPs along the detonation channel, air inlet throat, and into the extended plenum were utilized. During some testing, a high-speed pressure measurement (XTEL-190 Kulites) was taken in the throat at the same axial position of one of the CTAPs; however, after a few runs, it was found that the sensor was destroyed, and was subsequently removed for the remaining tests. Overall, having this arrangement of sensors allows for determining rotations in the plenum as well as longitudinal pulsing in the entire system by looking at the relative time histories measured by the various sensors.

B. Operating Conditions

A variety of H_2/air conditions were studied in this work for channel to inlet area ratios of 3 and 4. The cases that resulted in detonative operation are shown in Figure 3. Here we do not consider elevated inlet temperatures (T_2) and only consider ambient temperature cases. Not shown here are the combinations that did not result in sustained detonation operation for the sake of clarity and conciseness. A more generalized description of the operational characteristics of this geometry is presented in a companion work,[10] including operation at elevated inlet temperature.[14] This geometry saw a limited amount of operability at or above stoichiometric conditions which is why there are many more fuel-lean conditions tested and shown in Figure 3 than stoichiometric conditions. One of our previous studies observed that on our legacy axial-air inlet injectors, operability scales by the mass flux through the inlet throat instead of the mass flow.[11] Therefore, by utilizing the mass flux, we can better draw comparisons between cases at different area ratios in the analyses presented in subsequent sections.

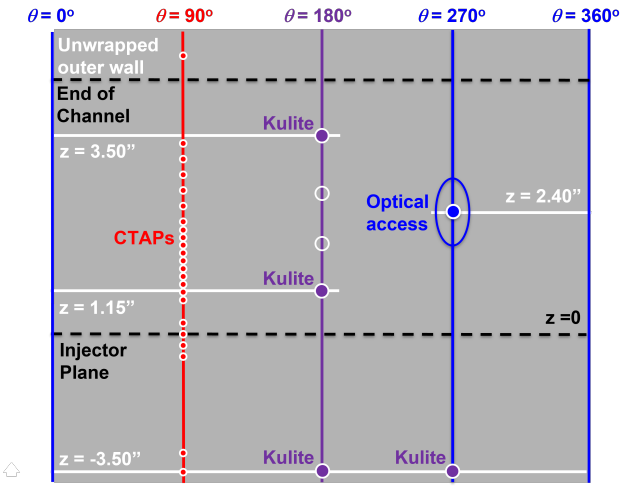

Figure 2. Unwrapped outer body showing different sensor positions relative to injector plane. High-speed pressure measurements (Kulites) are in purple, low-speed pressure measurements (CTAPs) are in red, and optical access is in blue.

III. Theorized Flowfield Representation

To better understand some of the dynamics present in a practical RDC, we seek to develop simplified representations and models of the various waves that originate from the propagation of one or more detonation waves in the RDC. These models can be used to better understand the operation of RDCs, as well as inform future designs. The traditional, simplified and unwrapped flowfield of an RDC showing the most important features is shown in the schematic diagram of Figure 4(a). The detonation wave propagates into a layer of height h of detonable mixture generated by the fuel/oxidizer injection system which flows downstream. The problem is two-dimensional; i.e., The flowfield develops into a constant gap channel. In a RDC the layer forms a closed loop, hence propagation is periodic. The layer is bounded on the upstream side by a wall, which contains the point of entry (injection) of fuel and oxidizer, and on the downstream side by the post-detonation products generated by the detonation wave propagating into the layer in the previous cycle. In this figure, if something (fluid particle, wave, etc.) is propagating towards the top of the figure, we say it is propagating downstream. Likewise, upstream propagating would refer to moving towards the bottom of the figure. A contact surface (slip line) separates the fresh layer from the downstream reacted layer. Upon the passage of the detonation wave, the slip line is deflected by the combined effect of a downstream propagating oblique shock (OS) and expansion fan (EF) that aids in injector recovery.[15] This is identical to the semi-bounded detonation wave with an inert gas boundary studied first by Sommers and Morrison[16] and later by Sichel and Foster.[17] This problem has been recently revisited by Fievisohn and Houim[3] with application to RDCs. In an ideal system, it can be assumed that the oblique shock interacts solely with combustion products, which are treated as a high-temperature inert. Previous work has treated detonations in RDCs as being semi-bounded in that the inlet/downstream side has been treated as a solid wall fresh reactants enter through.[15] For rocket-style injectors, that have a solid wall at the end of the detonation chamber and small holes for jet injection, the semi-bounded description is adequate. However, in an air-breathing RDC design with a low-loss inlet, such as the contoured axial air inlet considered in this work, the openness of the inlet throat more freely allows for the propagation of waves upstream into the plenum. It is theorized that this would effectively create a second free boundary on the inlet side that has not been previously considered in detail.

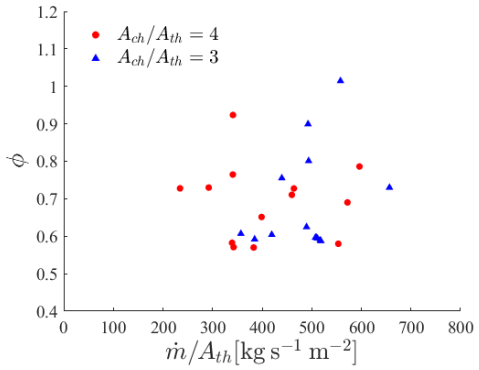

Figure 3. H_2/air detonative operating conditions for the different area ratios

A modified representation of the 2D steady flowfield in the RDC that removes the solid upstream (bottom)

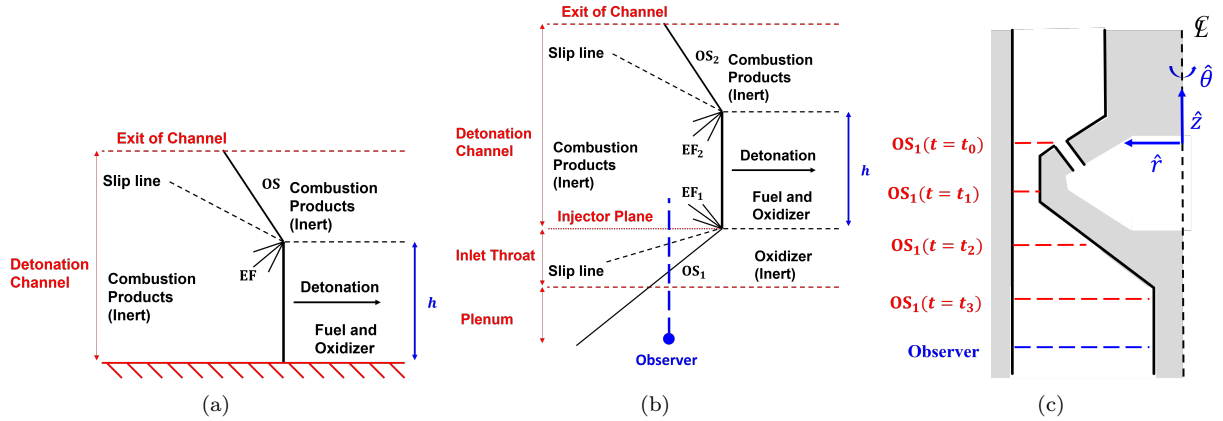

Figure 4. Ideal and simplified 2D steady flowfield in (a) rocket-style injector RDC and b) axial-air inlet (air-breathing) RDC. In case (b) the detonation wave is bounded on both ends by inert gases creating two free boundaries and two sets of oblique shocks (OS), slip lines, and expansion fans (EF). (c) Analogy to a quasi-1D, unsteady flow experienced by a fixed observer in plenum. Oblique shock is observed at different locations by the fixed observer at different times.

boundary is shown in Figure 4(b). In this case, the flowfield exhibits the theorized second free boundary on the upstream boundary. The detonation wave is treated as being bounded on both sides by inert gases, with each free boundary also having an oblique shock (OS), slip-line, and expansion fan (EF) centered at the point of intersection of the detonation wave, the oblique shock, and expansion wave. Like in the case of Figure 4(a), the inert gas downstream (top) is assumed to be post-combustion products with the added assumption that complete combustion occurs, infinitely fast reactions (i.e., infinitely thin detonation), and no downstream deflagration (either along the contact surface or other secondary combustion events) occurs due to complete combustion. These assumptions may not be representative of practical situations and may need to be rectified as the model is further developed to include non-ideal effects. The second inert gas upstream of the detonation wave is oxidizer (e.g., air) and originates from the axial inlet at the inlet conditions. Typically, the axial inlet is contoured; thus, the downstream free boundary develops through a variable-area (non-constant gap) channel. Red lines here denote important geometric locations along the axial distance, while black lines differentiate different thermodynamic states. The oblique shocks and expansion fans are grouped together such that OS_1 and EF_1 are those generated by the downstream free boundary, while OS_2 and EF_2 are for the upstream free boundary. As drawn in Figure 4(b), the area change in the inlet portion and incoming air velocity change have both been neglected – these will be considered further below. One consequence of a non-zero incoming axial air velocity is that the detonation wave would be slanted in the frame of reference drawn in Figure 4(b). Additionally, the area change and corresponding variation in incoming oxidizer velocity would lead to OS_1 being curved. Other waves and/or slip lines would also have curvature if these details are fully considered. However, solving for the proper shape of these waves is beyond the scope of this work. Thus, for now, we shall treat the flowfield as being represented by Figure 4(b) in a constant gap channel, with no inlet velocity and no tilt to the detonation wave.

In this work, we will often take the point of view of a fixed observer in the plenum when analyzing the problem. This fixed observer looks down the combustor across an infinitely thin azimuthal slice; i.e., it observers only a one-dimensional (1D) axial view of the problem. In Figure 4(b) the blue dot represents the fixed observer while the dashed blue line indicates the axis of the corresponding 1D problem constructed around the fixed observer. By considering the point of view or reference frame of the fixed observer, we effectively reduce the steady 2D flowfield to the quasi-1D problem shown in Figure 4(c). We now consider the detonation wave system to be unsteady so the detonation wave, oblique shock, and expansion fan propagate from left to right as shown in Figure 4(b) at equal speed. Because the fixed observer is stationary in space and observes the problem in a 1D sense only (axial view only), it perceives the lateral (rotational) motion of the oblique shock OS_1 as corresponding to a shock wave moving axially upstream (i.e., toward it). In other words, the position of OS_1 relative to the fixed observer changes over time only in the axial direction (along the blue dash line of Figure 4(b)). This is also shown in Figure 4(c) as the different dashed red lines. Thus, to the fixed observer, the OS_1 has an apparent axial velocity as the 1D shock wave propagates from the detonation towards the fixed observer. This apparent axial velocity is a result of the rotation of the

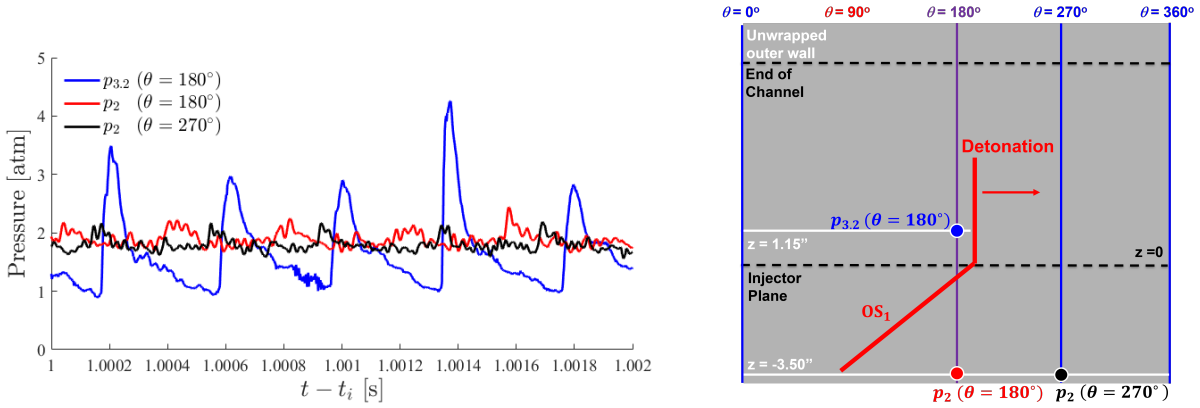

(a) (b)

Figure 5. (a) High-speed pressure measurements in channel ($p_{3.2}$) and in plenum (p_2) for case with: $\dot{m}/A_{th} = 399\ \mathrm{kg\,s^{-1}\,m^{-2}}$, $\phi = 0.65$, and $A_{ch}/A_{th} = 4$. (b) Example detonation and OS_1 propagation relative to sensor locations. Detonation wave first observed by blue trace, followed by red, and finally black before new detonation cycle begins.

oblique shock and its angle relative to the viewpoint of the fixed observer. It is in this context that we can assign an axial speed to the OS_1 to study its strength as well as constructing a quasi-1D shock tube model for evaluating the change in its strength across the area change of the inlet. This will be further developed subsequently. Here we focus only on the oxidizer inlet and at this time have not extended the analysis to the fuel injector. However, the methods presented in this work can also apply to the fuel injector, depending on the configuration, to analyze the disturbances that propagate into the fuel plenum.

IV. Analysis of Upstream Propagating Perturbations

A. Pressure Rise in Air Plenum

A sample pressure trace of a detonative case is shown in Figure 5 for an area ratio of 4, mass flux of 399 $\mathrm{kg\,s^{-1}\,m^{-2}}$, and an equivalence ratio of 0.65. This condition was arbitrarily chosen. In this figure, the blue trace ($p_{3.2}$ ($\theta = 180°$)) is taken within the detonation channel at the Kulite closest to the injector, while the red (p_2 ($\theta = 180°$)) and black (p_2 ($\theta = 270°$)) traces are both taken within the air plenum. To be consistent with literature, the channel is denoted as state (3.2) and the plenum as state (2).[1] Not shown here for clarity is the second detonation channel pressure measurement. The angles listed for each measurement are the same for those given to the measurement points in Figure 2 and the unwrapped outer wall is reproduced in Figure 5(b). The red and blue traces are at the same azimuthal location (shown by having the same θ), but spaced axially apart by about 118 mm (4.65"). The red and black traces are at the same axial location, but clocked azimuthally by 90°; hence the black trace has a $\theta = 270°$. The corresponding measurement points are shown in Figure 5(b) with the corresponding color to the time traces. While the plenum measurements see a pressure ratio much smaller than that in the detonation channel measurement, a discernible rise in both plenum measurements can be seen. Additionally, this pressure disturbance occurs at the same frequency as the detonation wave with a temporal offset between the clocked measurements in the plenum, which is consistent with the presence of the theorized upstream propagating shock, OS_1.

To study the temporal offsets in the pressure rises, the aft high-speed camera is used to track the detonation wave location in time. In the case shown in Figure 5(a), the detonation is observed to be spinning counter-clockwise. This would appear as traveling from left to right in Figure 2 as shown in Figure 5(b). We here arbitrarily define the start of the detonation cycle as the time the detonation wave passes the detonation channel sensor (blue dot in Figure 5(b)). At the moment that the detonation wave is at the blue dot, neither of the plenum sensors would observe the OS_1 as drawn. After some amount of time, the red measurement would be the first plenum measurement to observe the OS_1 being swept across it. The time difference can be explained as the time it takes the OS_1 to propagate through the throat and into the plenum. At an even later time, the OS_1 would finally arrive at the black measurement point. Thus, even though the pressure rise seen in the black trace in Figure 5(a) appears to be immediately before the

detonation, the OS_1 is from the first detonation cycle while the detonation in the channel marks the next detonation cycle. Therefore, when examining Figure 5, a detonation cycle consists of first the blue trace, then the red trace, and finally the black trace before the next cycle is observed with the arrival of a new detonation in the channel (blue trace).

B. Quantification of Oblique Shock Strength Penetrating The Inlet

The strength of the oblique shock penetrating the inlet and propagating into the plenum is defined as the pressure ratio across the wave as measured by the high-speed pressure sensors in the plenum. An algorithm has been constructed that examines all the individual detonation cycles in the high-speed pressure measurements. For each detonation cycle and for each pressure measurement, the points of the maximum and minimum pressure across the cycle are found and stored. This allows for a statistical measure of the pressure variation (ratio p_r) caused by the waves observed at different measurement points, as well as for finding the time between the peaks in the channel measurement and the plenum measurement (Δt). Here we denote a superscript of "+" to be point after the passage of the wave, which corresponds to the peak pressure across the cycle. Similarly, we denote a superscript of "-" to be the point before the arrival of the wave, which is typically the minimum pressure in the cycle. The pressure ratio ($p_{r,2}$) is defined as the ratio between these pressures according to:

$$p_{r,2} = \frac{p_2^+}{p_2^-} \tag{1}$$

By taking the average pressure ratio observed across the many detonation cycles ($\langle p_{r,2} \rangle$), a measure of the strength of the wave in the plenum for a given operating condition can be better explored. The average pressure ratios are shown in Figure 6. Here it can be seen that while smaller than the pressure ratios observed in the detonation channel, a finite pressure ratio is observed far upstream of the air inlet into the plenum. There is no immediately apparent relationship between the pressure ratio and either mass flux or equivalence ratio. On average, for a given air mass flux, the more open throat cases (triangles) have a larger pressure ratio than the more constrictive throat cases (circles). This could either indicate a greater coupling between the plenum and the detonation channel and/or fewer losses in the inlet throat that affect the penetration of OS_1 across the inlet into the plenum. Regardless, we can conclude that OS_1 in this system has a non-negligible strength in the plenum – between 20% to 40% – which may impact the integration of an RDC with upstream components, such as a compressor or isolator.

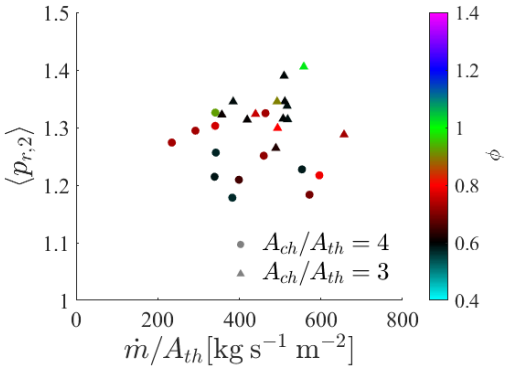

Figure 6. Average pressure ratio across wave observed in air plenum.

With the $\langle p_{r,2} \rangle$ values of Figure 6, further characterization of OS_1 can be done by estimating the *apparent* axial velocity of the wave (u_z) through normal shock relations. The velocity vectors describing the flow across OS_1 is shown in Figure 7 from the frame of reference of a fixed observer in the plenum and the frame of reference where the frozen detonation wave. For both frames of reference, we assume there is no radial variation to the properties of the wave in the plenum. Drawn in Figure 7 is the detonation wave and OS_1 similar to Figure 4(b), though we neglect all other flow features at this time.

First, we consider the point of view as a fixed observer in the plenum, Figure 7(a), which was illustrated previously in Figure 4(c). With respect to a fixed observer in the plenum, the oblique shock wave appears to propagate upstream into the plenum with an axial velocity (u_z) towards the fixed observer. This is the velocity a fixed observer in the plenum perceives OS_1 at an angle θ_1 to approach as the wave system rotates at a speed D. From geometric considerations of the apparent axial velocity and rotation speed, the angle between OS_1 and the axial axis, α, is:

$$\alpha = \tan^{-1}\left(\frac{D}{u_z}\right). \tag{2}$$

where

$$\alpha + \theta_1 = 90^\circ \tag{3}$$

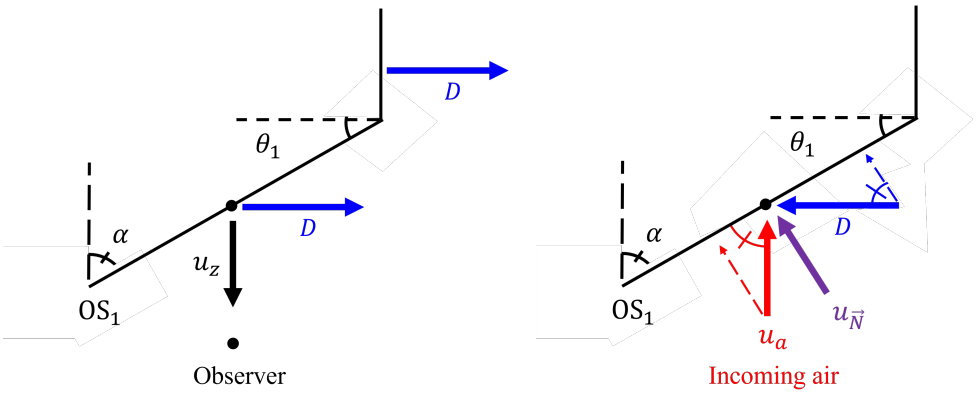

Figure 7. (a) A fixed observer in the plenum views the oblique shock propagating towards it with an apparent axial velocity of u_z due to rotation of wave system. See also Figure 4(c). (b) In the detonation frame of reference, the normal component of the incoming air vector ($u_{\vec{N}}$) is a combination detonation speed, D, and incoming air speed, u_a.

Meanwhile, in the lab frame, the air flows downstream towards the combustor with an axial velocity (u_a). Throughout this work, we will use the subscript "a" to indicate the velocity of the incoming air that is traveling towards the detonation channel. When transforming to the steady detonation wave-stationary frame of reference as shown in Figure 7(b), the resulting air vector now has an azimuthal component equivalent to the detonation wave speed (D). One of the assumptions imposed here is that the azimuthal component of the OS_1 propagation is equal to the measured detonation wave speed (D) at every axial location. To apply the normal shock relations, we find the normal component of the resultant air vector which is represented by $u_{\vec{N}}$. Using the geometry illustrated in Figure 7(b) and the angle found in Eq. 2, the normal velocity is found to be:

$$u_{\vec{N}} = u_a \sin(\alpha) + D\cos(\alpha) \tag{4}$$

$$= \sin(\alpha)\left(u_a + \frac{D}{\tan(\alpha)}\right) \tag{5}$$

$$= \sin(\alpha)(u_a + u_z) \tag{6}$$

This allows for the shock angle to become a function of u_z. The resulting normal shock pressure ratio is then:

$$\langle p_{r,2}\rangle = 1 + \frac{2\gamma}{\gamma+1}\left[\left(\frac{u_{z,2} + \langle u^-_{a,2}\rangle}{a_2}\right)^2 \sin^2(\alpha) - 1\right] \tag{7}$$

where α is also a function of u_z from Eq. 2.

In this analysis, the average incoming air velocity immediately prior to the passage of the wave ($\langle u^-_{a,2}\rangle$) is needed, which can be estimated by the measured pressure and temperature at the inlet from the known mass flow rate $\dot{m}_a$ according to:

$$\langle u^-_{a,2}\rangle = \frac{\dot{m}_a R T_2}{\langle p^-_2\rangle A_2}. \tag{8}$$

Utilizing these equations and the measured average pressure ratio in the plenum ($\langle p_{r,2}\rangle$), the axial velocity of OS_1 in the plenum at the sensor location can be numerically solved for. From the velocity the Mach number in the fixed observer frame and fluid frame (which we denote with superscript f) can be defined relative to the speed of sound of the incoming air:

$$M_{z,2} = \frac{u_{z,2}}{a_2} \tag{9}$$

$$M^f_{z,2} = \frac{u_{z,2} + u_{a,2}}{a_2} \tag{10}$$

The Mach number of the OS_1 in the fixed observer frame from this analysis for all the conditions tested in this work are shown in Figure 8(a). From Figure 8(a), it is found that to a fixed observer the OS_1 is traveling near the speed of sound of the incoming air in the plenum with a Mach number of about 1.1. To the incoming fluid element, the wave is coming in at about Mach 1.2 since the fluid element is traveling at about Mach 0.1 in the plenum. This is shown in Figure 8(b). It is expected that as the wave continues to propagate if the plenum was infinitely long, the wave would decay under the action of viscous forces until it was acoustic in nature; however, due to the finite size of the plenum, the wave likely did not decay entirely prior to reaching the end of the plenum in the tests conducted. It is theorized that if there were surfaces within the plenum that the wave could then reflect off of, the flowfield would be further complicated by the interactions of the waves penetrating into the plenum and reflections from previous cycles. This possibility is neglected in the current discussion as we consider a purely axial combustor, though it may be worth studying in the future.

C. Time of Flight Measurement of Upstream Propagating Disturbances

The time difference (Δt) between the observed peaks in the pressure traces measured in the channel and plenum, is another metric that can provide insight into the propagation of the theorized OS_1. Similar to the pressure rise, a peak finding algorithm is used to find the Δt between the peaks for each individual detonation cycle. We impose the assumption that the bottom of the detonation wave is azimuthally aligned with the part of the detonation that is measured using the pressure sensor in the channel. This assumption is imposed to equate the time difference between the pressure signals to the time that the OS_1 would take to propagate from the bottom of the detonation to the measurement location in the plenum in the unsteady quasi-1D reference frame. This is analogous to the time of flight of a shock within a 1D shock tube problem. Shown in Figure 9(a) are the average time differences ($\langle \Delta t \rangle$) for the various conditions tested. There is no discernible trend with air mass flux, equivalence ratio, or area ratio, with most of the data points falling within $\pm$ 10% of the average of 2.2E-4 s. We then normalize by the period of the detonation (τ_D) to provide a sense of scale, which is shown in Figure 9(b). The period of the detonation wave, shown in Figure 9(c), is calculated from the observed wave speed and the circumference of the midpoint in the detonation channel. Most of the normalized time of flight values ($\langle \Delta t \rangle / \tau_D$) are around 0.6. On average, the normalized time of flight increases linearly with increasing air mass flux, with no obvious difference between the two cases with different area ratios. This occurs despite the decrease in the detonation period with increasing air mass flux. This suggests that although the detonation wave sees an increase in speed with increasing mass flux, the OS_1 has less variation in its axial speed with air mass flux. Referring back to Figure 8(a), the estimated axial velocity of OS_1 varies by about 35 m/s across all conditions, which is an order of magnitude smaller than the change in the detonation wave speed, which is over 200 m/s between the lowest and highest air mass fluxes. Therefore, while the azimuthal speed of the OS_1 would vary with the detonation wave speed by being attached to the bottom of the wave, the axial velocity of OS_1 does not have a strong dependence on the strength of the detonation wave. This suggests that the wave angle α of OS_1 varies correspondingly to changes in wave speed (consider Eq. 2).

D. Fluid Residence Time of Plenum

Thus far, we have assumed that the incoming flow in the plenum/inlet is undisturbed prior to the passage of OS_1. This simplification removes any potential azimuthal velocity a fluid particle would have to maintain the quasi-1D approximation of purely axial flow. This assumption can be evaluated somewhat readily by taking the undisturbed velocity in the plenum computed previously ($u^-_{a,2}$) and applying area-velocity relations through the use of the sonic $\circledast$ state. The reference sonic area A^* can be computed from the high-speed pressure measurement according to:

$$A^* = A_2 \sqrt{\left(\frac{\langle u^-_{a,2} \rangle}{a_2}\right)^2 \frac{2}{\gamma+1}\left[1 + \frac{\gamma-1}{2}\left(\frac{\langle u^-_{a,2} \rangle}{a_2}\right)^2\right]^{\frac{-\gamma-1}{\gamma-1}}} \tag{11}$$

We then apply the assumption that the undisturbed flow along the variable area plenum and inlet is isentropic and quasi-one-dimensional. This neglects any radial velocity component due to the curve of the variable area geometry of the plenum and inlet. Within a quasi-one-dimensional approximation, while

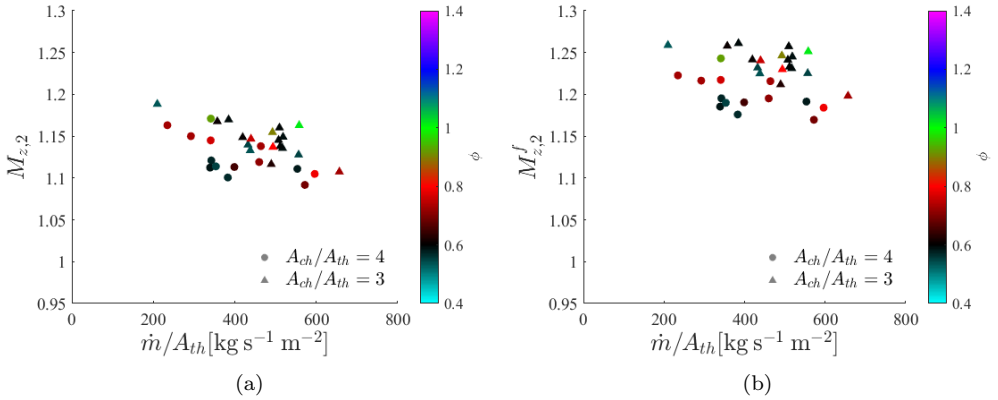

Figure 8. Estimated Mach numbers of OS_1 in plenum for (a) laboratory and (b) fluid particle frame of reference. Wave travels near acoustic speed upstream in laboratory reference frame at the measurement point.

accounting for any flow turning that may be imposed by the variable area geometry, the mid-line between the inner and outer walls is taken as the streamline ($\vec{S}$) along which the oxidizer fluid particles travel along. Therefore, instead of being purely a function of the axial location, z, we find the areas along this streamline and parametrize it by the curvilinear variable S, which itself is a function of axial and radial location.

In computing the stream-wise velocity of the undisturbed air, it was found that for all of the air mass fluxes that exhibited detonation, the undisturbed flow became choked in the inlet. This is explored further in a companion work that studied the impact of area blockage of the inlet.[10] This is not necessarily equivalent to having the entire inlet choked since computationally it has been observed that the inlet is momentarily un-choked.[18] It is likely that OS_1 is the mechanism by which the inlet becomes un-unchoked; however, this would result in the oblique shock propagating through a choked region and causing pressure disturbances upstream in the plenum. This is consistent with numerical simulations of RDC operation.[9] This suggests that, in this geometry, choking the flow is not be sufficient to prevent these upstream propagating disturbances.

After the flow became choked, the area began to increase again as the oxidizer would enter the detonation channel and the flow would expand. Because the choked conditions were met, this area increase could result in either the supersonic or the subsonic solution to the area Mach relation. For now, we chose the subsonic solution, though this assumption's impact on the results will need to be evaluated in the future. Integrating the velocity with respect to the distance along the streamline, the time it takes a fluid particle entering the base of the plenum to reach the fuel injector plane (S_{inj}) can be estimated. This quantity is referred to here as the residence time of the fluid particle τ_P:

$$\tau_P = \int_0^{S_{inj}} \frac{\mathrm{d}S'}{u_a(S)} \tag{12}$$

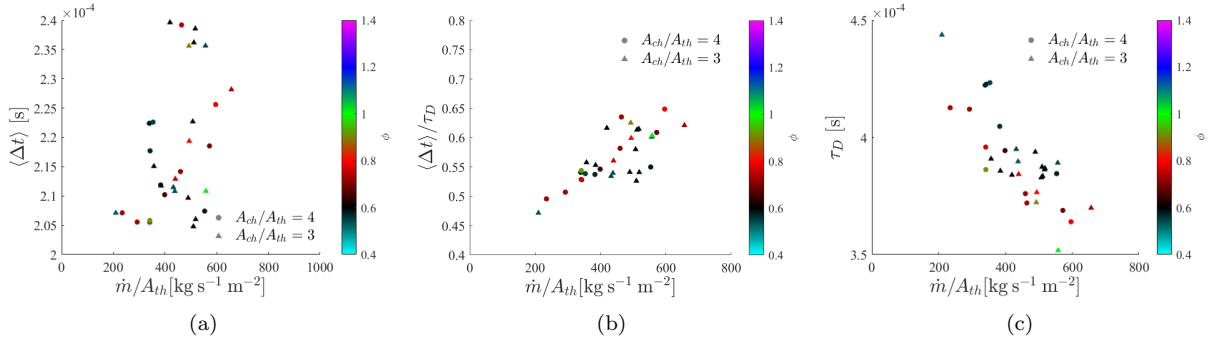

Figure 9. (a) Average time between pressure measurements taken in detonation channel and plenum ($\langle \Delta t \rangle$) does not vary much with mass flux; (b) ratio of $\langle \Delta t \rangle$ and the detonation period (τ_D) increases with mass flux; and (c) detonation period decreases with increasing mass flux.

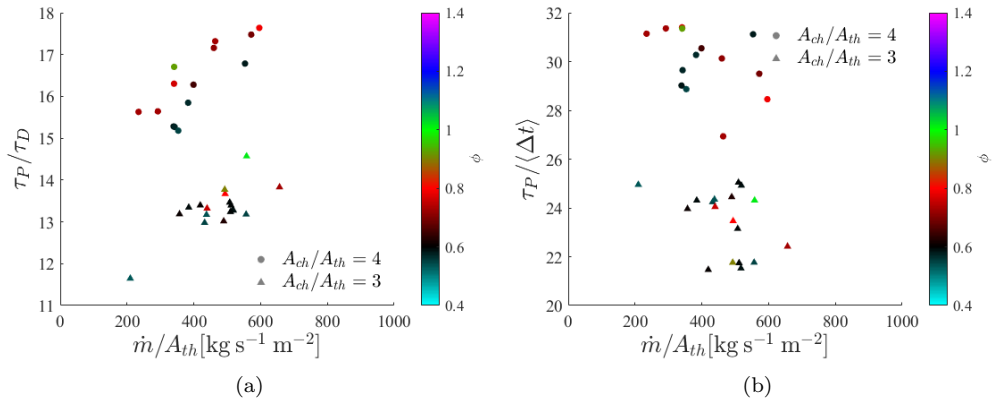

Figure 10. Time it takes for fluid particle to go from bottom of plenum to injector plane relative to (a) detonation period and (b) time for OS_1 to travel from injector to sensor in plenum. Fluid particle would see multiple shocks prior to entering the detonation channel.

The comparisons of this residence time to the detonation period and the experimental time of flight of the upstream propagating disturbance are shown in Figure 10(a) and Figure 10(b), respectively. From these figures, it is seen that the residence time is nearly an order of magnitude larger than both the detonation period and the time it takes for the OS_1 to travel into the plenum. Because of this, it seems very probable that a fluid element entering the plenum would experience multiple oblique shocks prior to arriving at the injector plane. However, at each oblique shock, the fluid particle should also encounter an upstream propagating expansion fan that turns the flow again to remove some of the azimuthal velocity that was imparted from the oblique shock. Despite the expansion waves, after each subsequent oblique shock encountered by the fluid particle would transfer more of the kinetic energy into thermal energy. As these effects compound, the OS_1 would have additional curvature caused by these varying properties, which is not captured by the present model. Furthermore, this would result in multiple drops of stagnation pressure across the plenum and inlet which may not be well characterized when the pressure gain across the RDC is defined.[6]

V. Modeling Upstream Propagation

A. Quasi-1D Shock Tube Analogy

While $\langle\Delta t\rangle$ could be used to calculate an average upstream propagation speed of OS_1 perceived by a fixed observer in the plenum, this average speed neglects the finer details of the propagation along the variable flow speed field imposed by the area change of the inlet throat. To account for the change in Mach number and corresponding pressure change through the converging section of the inlet, a more refined model describing the propagation of OS_1 in the air inlet is considered and developed next. This model will also allow for the evaluation of the response of and flow losses across the inlet throat.

Following the basic idea outlined initially, the refined model describes the axial propagation of OS_1 as perceived by a fixed observer in the plenum (see Figure 4(c)). We can leverage again the analogy that the rotating OS_1 (azimuthal motion) is perceived by a fixed observer in the plenum as a shock wave approaching the fixed observer at a speed $u_{\vec{S}}$ along $\vec{S}$. Then, the approach speed $u_{\vec{S}}$ is solely related by geometric consideration to the rotational speed D and the angle α of OS_1 according to Eq. 2. This suggests that the problem can be described in a simplified manner by considering the analogous problem of a shock wave propagating in a tube with a variable area (because of the inlet). The shock wave is supported by the pressure rise across the detonation wave moving at D. Therefore, we essentially treat the problem as a quasi-1D shock tube problem that includes the effect of area change in the propagation of the shock wave. This problem is similar to the problem considered by Chester,[19] Chisnell,[20] and Whitham.[21] The model is based on the following assumptions and simplifications to allow the use of the formulations proposed by Chester, Chisnell, and Whitham:

1. We consider only the component of the OS_1 propagation velocity along streamline $\vec{S}$ and neglect the azimuthal component.

2. The azimuthal component is unaffected by the axial area change and it is always equal to detonation wave speed D so that OS_1 remains attached to the bottom of the detonation wave.

3. The wave is planar and has no variation normal to the streamline $\vec{S}$.

4. Viscous losses along the wall are neglected.

5. The pressure downstream of the detonation wave in the channel remains constant; i.e., the pressure decrease and the recovery of the injector is not considered at this time.

6. Downstream propagating disturbances caused by reflections of upstream propagating waves due to area changes are neglected.

7. The shock propagates into a homogeneous fluid with constant pressure and density.

8. The shock propagates into quiescent flow (i.e., the motion of the air in the variable area inlet is neglected.) This assumption will later be relaxed by introducing a correction to account for the flow in the inlet.

The description of a shock propagating through an area change was formulated by Chester,[19] Chisnell,[20] and later Whitham[21] independently through different methods. Chester approached the problem by applying small perturbation theory for the flow behind a propagating shock wave caused by area change and linearized the equations of motion based upon a small area change assumption. Chisnell, on the other hand, produced a first-order relationship between area change and Mach number by decomposing the problem into many sequential shock tubes with small area changes. Though the derivation was different, the resulting relationship were functionally similar. Finally, Whitham presented a simplified derivation based on the integration of the compatibility equations along characteristic directions while imposing the Rankine-Hugoniot relations across the shock front to derive the same results of Chester and Chisnell. The end result is Eq. 13 which is an ODE that relates the change in shock propagation Mach number to change in cross-sectional area:

$$\frac{\mathrm{d}A}{A(S)} = -\left[\frac{2M_{\vec{S}}}{K(M_{\vec{S}})(M_{\vec{S}}^2-1)}\right]\mathrm{d}M_{\vec{S}} \tag{13}$$

where

$$K(M_{\vec{S}}) = 2\left[\left(1+\frac{2}{\gamma+1}\frac{1-\mu(M_{\vec{S}})^2}{\mu(M_{\vec{S}})}\right)\left(2\mu(M_{\vec{S}})+1+M_{\vec{S}}^{-2}\right)\right]^{-1} \tag{14}$$

and

$$\mu(M_{\vec{S}})^2 = \frac{(\gamma-1)M_{\vec{S}}^2+2}{2\gamma M_{\vec{S}}^2-\gamma+1} \tag{15}$$

Here we use $M_{\vec{S}}$ to denote the Mach number of the OS_1 propagation velocity parallel to $\vec{S}$ and it is assumed that this quantity is uniform on a surface normal to $\vec{S}$ at any given location. Based on the geometry of the variable area inlet and plenum, this Mach number could have a radial component in addition to the axial one at certain points in the flow.

When compared to experimental shock tube data, Chisnell[20] and Whitham[21] both found good agreement for a range of initial Mach numbers and for small instantaneous area changes. Large instantaneous area changes resulted in disturbance reflections becoming non-negligible.[20] To better match experimental shock tube data from Smith (which had a data-set with larger instantaneous area changes),[22] Milton expanded Eq. 13 by deriving a higher-order correction term to account for the Mach reflections that occur in the area change.[23] This results in Eq. 16:

$$\frac{\mathrm{d}A}{A(S)} = -\left[\frac{2M_{\vec{S}}}{K(M_{\vec{S}})(M_{\vec{S}}^2-1)}+\frac{\eta(M_{\vec{S}},A(S))}{M_{\vec{S}}}\right]\mathrm{d}M_{\vec{S}} \tag{16}$$

where $\eta(M_{\vec{S}},A(S))$ in Eq. 16 is defined as:

$$\eta(M_{\vec{S}},A(S)) = \frac{1}{2\gamma}\left[\left(\frac{\gamma(\gamma-1)}{2}\right)^{1/2}+1\right]\left(1-\frac{M_{\vec{S},0}^2}{M_{\vec{S}}^2}\right)+\frac{1}{2}\ln\left(\frac{A_0}{A(S)}\right) \tag{17}$$

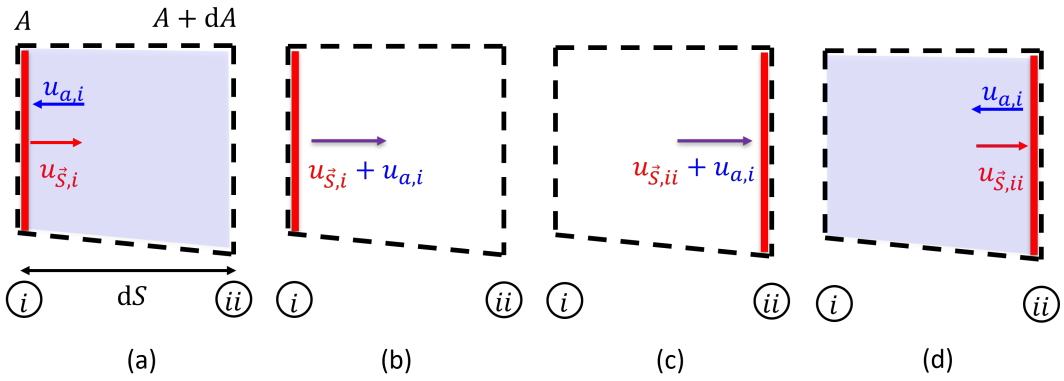

Figure 11. Diagrams showing the change of frame of reference to account for incoming air velocity in the estimation of the variation of shock Mach number. a) OS_1 propagates into fluid with motion $u_{a,i}$ in the laboratory frame. b) Frame of reference transformed such that the incoming air is at rest. c) The shock strength (with Mach number in fluid at rest frame) changes due to area change. d) Convert back to laboratory reference frame to get the new velocity of OS_1.

and it is the additional term (compare to Eq. 13) that arises when changes along the characteristic lines due to wave reflection at points of variable area are included. The subscript "0" denotes the conditions of the main shock wave; i.e., the initial conditions.

The use of Eq. 16 over Eq. 13 is advantageous because of the better agreement with experimental data for cases with large area changes. Additionally, Milton found that the extra correction term allowed for a better agreement to experiments at lower Mach numbers.[23] This is especially relevant as we have seen that M_z is approaching the acoustic limit in the large plenum from Figure 8(a).

As noted previously, the formulation of Eqs. 13 or 16 only accounts for the propagation of shock waves into a quiescent fluid. This simplification ignores the large velocities of the incoming fluid in the variable area inlet, especially as the inlet throat is approached. To account for the speed of the incoming fluid, next, we introduce the following correction. With reference to the diagram of Figure 11, we consider the propagation of the shock wave across an infinitesimally thin slice (length dS) of the hypothetical quasi-1D shock tube of width dS. Over this slice the area varies by dA as the wave propagates from state ⓘ to state ⓘⓘ. Initially, the wave enters this slice with a velocity $u_{\vec{S},i}$ and as a consequence of the area change, it leaves at a different speed $u_{\vec{S},ii}$. The difference in the speed of the incoming air at state ⓘ ($u_{\vec{S},i}$) and at state ⓘⓘ ($u_{\vec{S},ii}$) is assumed to be small (though non-zero) over the infinitesimal distance dS. For now, we make the assumption that the flow is purely along the streamline and has not been turned by an oblique shock or expansion wave originating from a previous cycle. However, this last assumption is likely incorrect because Figure 10 has shown that the residence time of a fluid particle is many times the rotational time of the detonation wave. The small variation assumption leads to the simplification that the region between states has a constant air velocity that is equal to the air velocity at state ⓘ ($u_{a,i}$). Similarly, the speed of sound between states is equal to the speed of sound at state ⓘ (a_i). By transforming from the laboratory frame of reference to the fluid particle frame of reference (which we again denote with superscript f), the problem then becomes a shock propagating into quiescent flow similar to the formulation used in Eq. 16. The relative Mach number of the shock then can be defined as:

$$M^f_{\vec{S},i} = \frac{u_{\vec{S},i} + u_{a,i}}{a_i} \tag{18}$$

Applying Eq. 16 over this small region allows for the determination of the change in the relative strength of the wave, and thus the shock propagation Mach number corrected for the effect of approach fluid velocity ($M^f_{\vec{S},ii}$) is found. Once this is done, the velocity of the shock in the fixed observer frame of reference is computed by changing back from the fluid frame of reference into the fixed observer frame of reference:

$$u_{\vec{S},ii} = a_i M^f_{\vec{S},ii} - u_{a,i} \tag{19}$$

This process is then repeated for every subsequent dS step to capture the effects of having a variable velocity of the incoming fluid flow.

Equation 16 indicates that the shock Mach number is a function of the local area, $M_{\vec{S}}(A)$, which in turn is a function of position, $A(S)$. Thus, applying the chain rule to the derivative of $M_{\vec{S}}$ with respect to position, we can write that:

$$\frac{\mathrm{d}M_{\vec{S}}}{\mathrm{d}S} = \frac{\mathrm{d}M_{\vec{S}}}{\mathrm{d}A}\frac{\mathrm{d}A}{\mathrm{d}S} \tag{20}$$

which is a function of S only. Then, a shock propagation Mach number distribution as a function of location along $\vec{S}$ can be solved for by numerical integration according to:

$$M_{\vec{S}}(S) = \int_0^S \frac{\mathrm{d}M_{\vec{S}}}{\mathrm{d}S}\mathrm{d}S' \tag{21}$$

Given a known geometry of the RDC plenum and inlet, the spatial distribution of $M_{\vec{S}}$ is dependant upon the initial conditions; i.e., given A_0 and $M_{\vec{S},0}$. Here we make the assumption that the bottom of the detonation wave, where OS_1 originates, is at the fuel injection plane (i.e., the axial plane where the fuel injectors are located), which is located at S_{inj} along the streamline. Currently, we cannot assess this assumption experimentally in the RDC geometric configuration considered, but this assumption is consistent with observations made in our optically accessible RDC.[24] This assumption allows us to express the initial conditions as follows:

$$M_{\vec{S},0} = M_{\vec{S}}(S = S_{inj}) \tag{22}$$

$$A_0 = A(S = S_{inj}) \tag{23}$$

The initial shock axial Mach number ($M_{\vec{S},0}$) is needed to integrate Eq. 21, but it may not be readily known, unless it is measured directly, or estimated by solving the lower triple point (where OS_1, EW_1 and the detonation wave meet) using an approach similar to that of Sichel and Foster[17] – this will be left for future work. Therefore, to bound the problem, Eq. 21 must be solved with a value of $M_{\vec{S},0}$ that is consistent with an imposed constraint. Here we take the appropriate constraint to be the measured time of flight, $\langle\Delta t\rangle$, measured between the high-speed pressure transducers located in the plenum. We make the assumption that the detonation is axially straight within the channel such that it reaches at the same time both the pressure transducer in the channel and the fuel injection plane at the same azimuthal location. Therefore, we define $\Delta t'$ (the $\prime$ is used to differentiate from the experimentally measured value) as the time it takes the OS_1 to go from the injection plane (A_0 at S_{inj}) to the pressure transducer in the plenum (S_p) by integrating $M_{\vec{S}}(S)$ across the streamline. Thus we write:

$$\Delta t' = \int_{S_{inj}}^{S_p} \frac{\mathrm{d}S'}{M_{\vec{S}}(S)a(S)} \tag{24}$$

The local speed of sound ($a(S)$) was computed assuming that the stagnation temperature everywhere in the undisturbed flow is equal to the measured plenum temperature (T_2):

$$a(S) = \sqrt{\gamma RT(S)} \tag{25}$$

$$= \sqrt{\frac{\gamma RT_2}{1 + \frac{\gamma-1}{2}M_{\vec{S}}^2(S)}} \tag{26}$$

With a known $A(S)$ and γ along with an assumed A_0, $\Delta t'$ then only depends on $M_{S,0}$. Therefore, Eq. 21 can be iteratively solved for using different $M_{\vec{S},0}$ values until the modeled time of flight estimated matches the one measured experimentally (i.e., $\Delta t' = \langle\Delta t\rangle$). This gives the sought estimate of the propagation axial Mach number through the inlet and plenum

Sample results from this analysis is shown in Figure 12 for the same case shown in Figure 5: $\dot{m}/A_{th} = 399\ \mathrm{kg\ s^{-1}\ m^{-2}}$, $\phi = 0.65$, and $A_{ch}/A_{th} = 4$. In Figure 12(a) the Mach number is evaluated in the fixed observer frame of reference, while in Figure 12(b) it is expressed in the frame of reference where the fluid particle is at rest. The difference between these two distributions then is the velocity distribution of the downstream propagating oxidizer. Here the fuel injector plane is set to be at the origin of the x-axis, and the plenum pressure transducer is at the end of the shown curves. In the fluid particle reference frame, the wave accelerates through the area contraction in the inlet before slowing down once the larger plenum is reached. These results are expected from the negative sign in Eq. 16. Due to the high speeds of the oxidizer in the

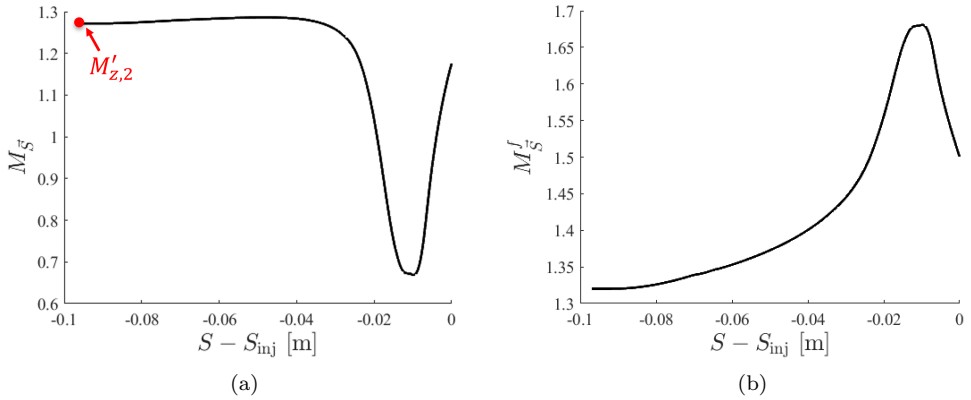

Figure 12. Variation of Mach number along streamline in (a) fixed observer and (b) fluid particle frame of reference. Difference between curves is fluid particle velocity. Fluid particle experiences different shocks depending on position in plenum/inlet.

inlet, to the fixed observer, the OS_1 actually appears to slow to subsonic speeds while traveling through the inlet before becoming supersonic in the plenum. It might appear that it is subsonic, but in reality, the wave is supersonic as viewed by the fluid.

This model was run for all of the detonative conditions in this work. The endpoint of the distribution in Figure 12(a) is labeled as $M'_{z,2}$ to draw comparison to the experimental estimates of the axial Mach number in the plenum discussed in a previous section since the streamline is purely axial at the sensor location. Again the $\prime$ is used to differentiate the model results from the experimental estimates. The modeled plenum Mach numbers in the plenum for all the considered cases are shown in Figure 13(a). Effectively there is a constant value of $M'_{z,2}$ (of about 1.25) across all the operating conditions considered. Similarly, differences in throat area do not have a definitive impact on $M'_{z,2}$ since both area ratios resulted in the nearly constant $M'_{z,2}$ value.

Figure 13(b) compares the modeled Mach numbers to those computed using the measured pressure ratio in the plenum – see Section IV.B. – and reveals a discrepancy between the two values since all the data points are above the 1:1 dashed line. This indicates that the model predicts in the plenum a faster-moving wave than what is estimated from the pressure ratios; thus, it also overpredicts the pressure raise that would be observed in the plenum. A possible explanation for this large discrepancy is the assumption imposed that the pressure downstream of the shock in the quasi-1D shock tube is constant. This assumption ignores the pressure relief caused by the upstream propagation expansion wave. With a decrease in the downstream pressure, the upstream propagating wave would travel at lower speeds. If described in the fixed observer frame, this effect results from the interaction of an upstream propagating expansion wave that slows the shock wave, while in the detonation wave frame this effect results from the upstream propagation wave curving the OS_1. Further improvements to this model could try to capture these additional phenomena and interactions, which may result in a better prediction of the speed and strength of the upstream propagating shock in the plenum. Nevertheless, both methods suggest that the wave is approaching acoustic speeds in the plenum.

B. Thermodynamic State Considerations

One of the implications of having an oblique shock traveling upstream into the plenum is the potential changes of the thermodynamic state of the flow entering into the combustor that the oblique shock may cause. In addition, the presence of an upstream propagating oblique shock contributes to the losses (e.g., stagnation pressure losses) experienced at the inlet. As we have seen from the model results, relative to the incoming fluid particles, that the oblique shock appears stronger at different locations along the streamline (Figure 12(b)). For example, a fluid particle at the throat of the inlet, where it is nearly at sonic speed, experiences a stronger incoming shock wave than a fluid particle in the plenum, which is moving at a much slower speed. Hence, (stagnation pressure) losses experienced by fluid particles at the inlet throat are larger than those experienced by fluid particles further upstream from the inlet throat. Additionally, because the fluid transit time through the inlet is much larger than the rotational time of the detonation wave, a fluid

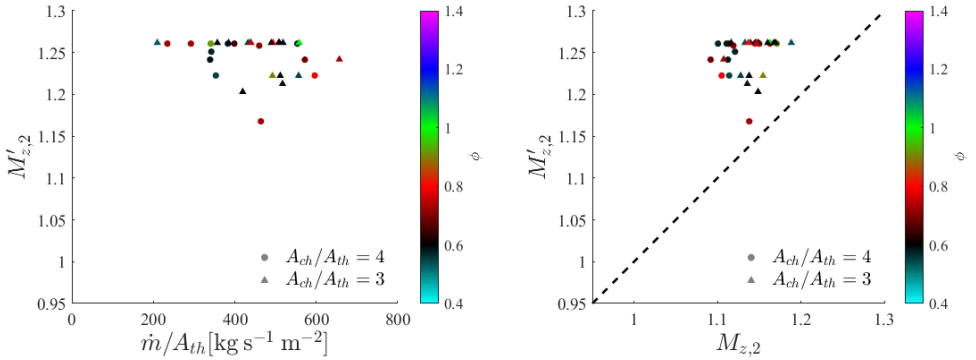

Figure 13. (a) Modeled streamline Mach number of OS_1 in plenum ($M'_{Z,2}$) as viewed in the laboratory reference frame; and (b) $M'_{Z,2}$ agrees favorably with computed Mach number based upon measured pressure ratio ($M_{Z,2}$).

element emerging from the inlet experiences several passages of OS_1, hence it undergoes multiple loss events.

Consider now that the fill region enables the detonation wave to have height h above the fuel injector plane. At the moment that the detonation wave would pass through the fresh mixture, the fixed observer would see what is shown in Figure 14. The light blue shaded region is the current detonation cycle fill height (subscript i), while the fluid that would comprise the next detonation cycle's (subscript $i-1$) fill height is the darker blue shaded region beneath the injector plane. At the moment that the fixed observer would watch the detonation wave consume the fresh mixture, the OS_1 (the solid red line) would separate these two shaded regions. The fluid particle that is at the bottom of the dark blue shaded region will be the fluid particle that is at the injection plane for the next cycle, while the top of the shaded region will be a distance h away from the injection plane. Considering unsteadiness, the fluid particles in the dark blue would continue to propagate downstream as the OS_1 propagates upstream. However, based upon what was seen in Figure 12(b), different points along the blue shaded region would see different shock strengths due to the area change affecting the speed of the wave and oxidizer. In other words, the bottom part of the next fill region sees a different shock than the top from this reference point. This effectively creates different thermodynamic states all along the fill region that the detonation propagates into. The effect on the detonation wave is unknown at this time, but in future work, we will examine these variations as the quasi-1D shock tube model is refined to include the release of pressure downstream of the detonation wave.

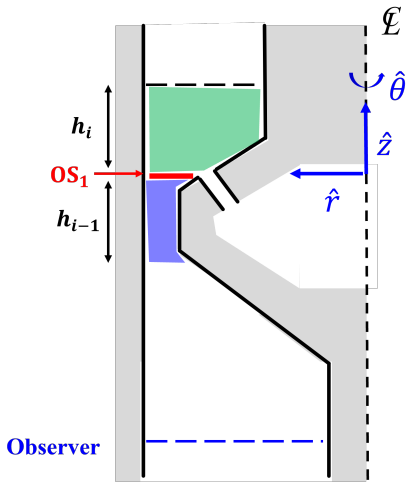

Figure 14. Average pressure ratio across wave observed in air plenum.

VI. Conclusion

A H_2/air operated RDC with an axial air inlet was tested at two different ratios of the channel area to the inlet throat area. For each area ratio, various air mass fluxes and equivalence ratios were tested. High-speed pressure measurements in the detonation channel and far upstream in the plenum were used to characterize the wave dynamics within the RDC. Experimentally, we observed that there were pressure disturbances that penetrated into the inlet despite the inlet being choked. From constructing a simplified version of the flowfield within a RDC having a free boundary of an inert gas (the oxidizer), an extension to what has been done by Fievisohn and Yu[15] previously, we conclude that the measured pressure disturbances are caused by an upstream propagating oblique shock that goes through the inlet and into the plenum.

To analyze the strength of the upstream propagating shock, a statistical measurement of the pressure ratio across the disturbances in the plenum was computed. For the conditions tested, the oblique shock caused a momentary increase in pressure of about 20%-40% of the undisturbed value. These non-negligible

disturbances could be problematic once a RDC is integrated with a compressor or isolator. By applying shock relations to the measured pressure ratios, the axial Mach number of the oblique shock propagating towards a fixed observer in the plenum (i.e., the pressure transducer) was estimated. Relative to the incoming oxidizer, this axial Mach number was on average about 1.22, while in the fixed observer frame of reference, the wave is moving slower at about 1.12 the speed of sound. Thus, even though the pressure ratio is non-negligible, it appears that the oblique shock is approaching the acoustic limit in the plenum.

In addition to the statistical measurement of the pressure rise, a statistical measurement of the time difference between the time the channel transducer observes the arrival of the detonation wave and that the plenum transducer observes the arrival of the oblique shock was conducted. This time difference quantifies the effective time of flight a perturbation originates in the channel and propagates to a fixed point of observation in the plenum. This time of flight is found to be on the order of the detonation period, though as the detonation period decreased with increasing air mass flux, the time of flight remained relatively constant. By comparing the detonation period to the time it would take a fluid particle to travel from the base of the plenum to the fuel injection plane, it was found that the detonation period was an order of magnitude smaller. This would result in a fluid particle experiencing multiple interactions with the rotating oblique shock as multiple periods would occur before entering the detonation channel.

A model of the upstream propagating oblique shock through the area change of the inlet was developed and presented by drawing an analogy to a quasi-1D shock tube with area change. The effects of the oxidizer flow in the opposite direction of the propagation of the oblique shock are preserved by repeatedly changing to the fluid frame of reference while integrating the model. In the fixed observer frame, the oblique shock is again found to be approaching the acoustic limit, though the results of the model predict slightly higher speeds (an average Mach number of 1.25) than those estimated based upon the experimentally measured pressure ratio. In the fluid frame of reference, the strength of the oblique shock increased from the area convergence before decreasing in the plenum. This suggests that possibility that different fluid particles entering into the detonation channel experienced upstream propagating shocks of different strength, thereby creating variations in the thermodynamic state within the fresh fill region just.

Acknowledgments

This paper is based on work supported by the DOE/NETL University Turbine Systems Research award number DOE FE0031228 with Mark Freeman as technical monitor. Further support to A.F. was provided by the Department of Defense (DoD) through the National Defense Science & Engineering Graduate Fellowship (NDSEG) Program.

References

[1]Brophy, C. M. and Codoni, J., "Experimental Performance Characterization of an RDE Using Equivalent Available Pressure," *AIAA Propulsion and Energy 2019 Forum*, Aug 2019.

[2]TenEyck, Joshua, A., "Determination of Effective Available Pressure of a Rotating Detonation Engine," 2019.

[3]Fievisohn, R. T., Hoke, J., and Holley, A. T., "Equivalent Available Pressure Measurements on a Laboratory RDE," *AIAA Scitech 2020 Forum*, Jan 2020.

[4]Bach, E., Paschereit, C. O., Stathopoulos, P., and Bohon, M., "RDC Operation and Performance with Varying Air Injector Pressure Loss," *AIAA Scitech 2020 Forum*, Jan 2020.

[5]Bennewitz, J. W., Bigler, B., Danczyk, S., Hargus, W. A., and Smith, R. D., "Performance of a Rotating Detonation Rocket Engine with Various Convergent Nozzles," *AIAA Propulsion and Energy 2019 Forum*, Aug. 2019.

[6]Kaemming, T. A. and Paxson, D. E., "Determining the Pressure Gain of Pressure Gain Combustion," *2018 Joint Propulsion Conference*, July 2018.

[7]Fotia, M., Hoke, J., and Schauer, F., "Propellant Plenum Dynamics in a Two-dimensional Rotating Detonation Experiment," *52nd Aerospace Sciences Meeting*, Jan. 2014.

[8]Anand, V., George, A. S., and Gutmark, E., "Amplitude modulated instability in reactants plenum of a rotating detonation combustor," *International Journal of Hydrogen Energy*, Vol. 42, No. 17, apr 2017, pp. 12629–12644.

[9]Schwer, D. and Kailasanath, K., "Feedback into Mixture Plenums in Rotating Detonation Engines," *50th AIAA Aerospace Sciences Meeting including the New Horizons Forum and Aerospace Exposition*, jan 2012.

[10]Shepard, J., Feleo, A., and Gamba, M., "Effects on Inlet Area Ratio on Operability of Axial Air Inlet Rotating Detonation Combustor," *AIAA Propulsion and Energy 2021 Forum*, 2021.

[11]Chacon, F., Feleo, A., and Gamba, M., "Impact of Inlet Area Ratio on the Operation of an Axial Air Inlet Configuration Rotating Detonation Combustor," *AIAA Propulsion and Energy 2019 Forum*, 2019.

[12]Duvall, J., Chacon, F., Harvey, C., and Gamba, M., "Study of the Effects of Various Injection Geometries on the Operation of a Rotating Detonation Engine," *2018 AIAA Aerospace Sciences Meeting*, Jan. 2018.

[13]Feleo, A., Chacon, F., and Gamba, M., "Effects of Heat Release Distribution on Detonation Properties in a H2/Air Rotating Detonation Combustor from OH* Chemiluminesence," *AIAA Propulsion and Energy 2019 Forum*, 2019.

[14]Feleo, A., Shepard, J., and Gamba, M., "Elevated Inlet Temperature Effects on the Operation of a Rotating Detonation Combustor," *AIAA Propulsion and Energy 2021 Forum*, 2021.

[15]Fievisohn, R. T. and Yu, K. H., "Steady-State Analysis of Rotating Detonation Engine Flowfields with the Method of Characteristics," *Journal of Propulsion and Power*, Vol. 33, No. 1, Jan. 2017, pp. 89–99.

[16]Sommers, W. P. and Morrison, R. B., "Simulation of Condensed-Explosive Detonation Phenomena with Gases," *Physics of Fluids*, Vol. 5, No. 2, 1962, pp. 241.

[17]Sichel, M. and Foster, J., "The ground impulse generated by a plane fuel-air explosion with side relief," *Acta Astronautica*, Vol. 6, No. 3-4, March 1979, pp. 243–256.

[18]Sato, T., Chacon, F., White, L., Raman, V., and Gamba, M., "Mixing and detonation structure in a rotating detonation engine with an axial air inlet," *Combustion Institute*, Vol. 38, No. 3, 2021, pp. 3769–3776.

[19]Chester, W., "CXLV. The quasi-cylindrical shock tube," *The London, Edinburgh, and Dublin Philosophical Magazine and Journal of Science*, Vol. 45, No. 371, Dec. 1954, pp. 1293–1301.

[20]Chisnell, R. F., "The motion of a shock wave in a channel, with applications to cylindrical and spherical shock waves," *Journal of Fluid Mechanics*, Vol. 2, No. 3, May 1957, pp. 286–298.

[21]Whitham, G. B., "On the propagation of shock waves through regions of non-uniform area or flow," *Journal of Fluid Mechanics*, Vol. 4, No. 04, Aug. 1958, pp. 337.

[22]Smith, L., of Scientific Research, U. S. O., and 2, D. N. D. R. C. D., *Photographic Investigation of the Reflection of Plane Shocks in Air: Final Report*, OSRD report, Division 2, National Defense Research Committee of the Office of Scientific Research and Development, 1945.

[23]Milton, B. E., "Mach Reflection Using Ray-Shock Theory," *AIAA Journal*, Vol. 13, No. 11, Nov. 1975, pp. 1531–1533.

[24]Chacon, F. and Gamba, M., "Development of an optically accessible continuous wave Rotating Detonation Engine," *2018 Joint Propulsion Conference*, American Institute of Aeronautics and Astronautics, jul 2018.